CrossMark

ROYAL
AERONAUTICAL
SOCIETY

REGULAR PAPER

Three-dimensional finite-time guidance law based on sliding mode adaptive RBF neural network against a highly manoeuvering target

G. Wu, K. Zhang and Z. Han

School of Astronautics, Northwestern Polytechnical University, Xi'an, China
E-mail: wugang88@mail.nwpu.edu.cn

Abstract
In order to intercept a highly manoeuvering target with an ideal impact angle in the three-dimensional space, this paper promises to probe into the problem of three-dimensional terminal guidance. With the goal of the highly target acceleration and short terminal guidance time, a guidance law, based on the advanced fast non-singular terminal sliding mode theory, is designed to quickly converge the line-of-sight (LOS) angle and the LOS angular rate within a finite time. In the design process, the target acceleration is regarded as an unknown boundary external disturbance of the guidance system, and the RBF neural network is used to estimate it. In order to improve the estimation accuracy of RBF neural network and accelerate its convergence, the parameters of RBF neural network are adjusted online in real time. At the same time, an adaptive law is designed to compensate the estimation error of the RBF neural network, which improves the convergence speed of the guidance system. Theoretical analysis demonstrates that the state and the sliding manifold of the guidance system converge in finite time. According to Lyapunov theory, the stability of the system can be guaranteed by online adjusting the parameters of RBF neural network and adaptive parameters. The numerical simulation results verify the effectiveness and superiority of the proposed guidance law.

Nomenclature

RBF	radial basis function
LOS	line of sight
PNGL	proportional navigation guidance law
TPNGL	true proportional navigation guidance law
GTPNGL	generalized true proportional navigation guidance law
PPNGL	pure proportional navigation guidance law
IPNGL	ideal proportional navigation guidance law
MPC	model predictive control
SMDO	sliding mode disturbance observer
ISS	input to state
NTSMGL	nonlinear terminal sliding mode guidance law

1.0 Introduction

In the past few decades, proportional navigation guidance law (PNGL) has been the widely used homing missile interception strategy, because of its advantages such as simple calculation, robustness and practicability [1]. References [2–6] also proposed some variation forms of proportional navigation guidance law (PNGL), such as adaptive motion camouflage proportional guidance law, true proportional

navigation guidance law (TPNGL), generalized true proportional navigation guidance law (GTPNGL), pure proportional navigation guidance law (PPNGL) and ideal proportional navigation guidance law (IPNGL), and discussed their advantages and disadvantages. In the terms of different requirements and constraints, especially for manoeuvering targets and impact angle constraints, scholars have put forward many improved PNGL forms, while PNGL is more suitable for interception of non-manoeuvering targets. When intercepting targets with strong manoeuverability, the performance of the PNGL algorithm will be reduced. This defect promotes the research of advanced control method and its application in the design of the missile guidance system.

In recent years, some progress has been made in the research of three-dimensional guidance law design. In Ref. [7], a three-dimensional nonlinear trajectory tracking guidance law, on the back of differential geometry of space curves, got into the public scene. The guidance law makes the aircraft converge to the ideal path of a given general shape and move along it without restrictions on the initial position and velocity. In Ref. [8], an adaptive three-dimensional PNGL based on convex optimisation is proposed to for the problem of LOS angle and acceleration constraints. By solving the optimisation problem, the proportional guidance gain is obtained. In Ref. [9], based on multivariable control design method, a suboptimal three-dimensional guidance law with end-angle constraint is proposed for intercepting unknown manoeuvering targets. The guidance law is essentially a compound control method, which is a combination of standard continuous model predictive control (MPC) and adaptive multivariable sliding mode disturbance observer (SMDO). They are used to track the optimal LOS angle of non-manoeuverable targets and to estimate the unknown manoeuvering information of compensated targets online. In Ref. [10], based on the finite time input-to-state (ISS) theory, a three-dimensional nonlinear guidance law with finite time convergence is proposed in the absence of linearisation hypothesis and target acceleration estimation. The line-of-sight angular rates can be stabilised within a small convergence range in a finite time. In Ref. [11], a nonlinear suboptimal guidance law, which minimises an integrated quadratic performance index, appears. To simplify the guidance algorithm, theta-D method is used to replace solving Hamilton-Jacobi-Bellman equation of the nonlinear system. In Ref. [12], a three-dimensional guidance law was designed based on the feedback linearisation method for the problem of missile intercepting manoeuvering targets at any initial heading. In Ref. [13], a guidance law based on computational geometry of three-dimensional collision time and angle constraints is introduced. The guidance law allows the missile to move to the target along a specific trajectory. The collision line forms a direction consistent with the expected collision angle, so as to meet the collision angle constraint, and the impact time is controlled by adjusting the length of the trajectory. In Ref. [14], based on sliding mode control theory and backstepping design technology, a robust guidance law for three-dimensional manoeuvering target interception considering autopilot dynamics and terminal angle constraints is raised. A second-order adaptive sliding mode observer is used to estimate target manoeuver, so that the missile can accurately intercept the target in a limited time. In Ref. [15], based on the approach of discrete-time partial stabilisation, a robust guidance law for intercepting manoeuvering targets in a three-dimensional environment is presented.

For the past few years, sliding mode variable structure control theory has been widely used in guidance law design because of its good robustness to external disturbances and parameter perturbations [16]. However, most of the developed sliding mode guidance laws are only exponentially or asymptotically stable, and usually only when the time is close to infinity, will the designed sliding surface tend to zero or its very small neighborhood [17]. Generally speaking, the flight time of missile terminal guidance is very short, so the design of guidance law should consider the finite time convergence control method. In recent years, novel sliding-mode guidance law with finite time convergence has been proposed, which includes second-order sliding mode guidance law [18, 19], fast terminal sliding-mode guidance law [20], nonsingular terminal sliding-mode guidance law [21–23], output feedback continuous terminal sliding mode guidance law [24], adaptive second-order nonsingular terminal sliding mode guidance law [25], integral sliding mode guidance law [26, 27] and super-twisting integral sliding mode guidance law [28].

However, chattering of sliding mode control is a tricky problem, which will cause serious harm to guidance system. This undesirable phenomenon is caused by the discontinuous switching function in

the guidance law. To solve this problem, it is common to approximate discontinuous sign functions with continuous sigmoid functions [29]. However, there are still the following disadvantages. (1) The sigmoid function cannot guarantee the finite time convergence of the sliding mode variables in the presence of external perturbations. (2) The sigmoid function cannot make the sliding variable drive to zero. (3) The sigmoid function is not directly considered in stability analysis.

So far, the techniques of disturbance and uncertainty estimation such as nonlinear disturbance observer [30], nonhomogeneous disturbance observer with finite time convergence [31], fixed-time convergence disturbance observer [32], extended high gain observer [33], robust nonlinear disturbance observer [34], extended state observer [35, 36, 37] and nonlinear robust H-infinity observers [38], have made important contributions to the treatment of many uncertain disturbances in guidance systems.

At present, although there are a large number of research results for the design of three-dimensional guidance law, the following problems still need to be solved: (a) Under the condition that the overload capability of the missile does not take an obvious advantage, it can intercept the large manoeuvering target accurately; (b) accurately estimate the disturbance of the guidance system caused by the target manoeuver; (c) line-of-sight angle and line-of-sight angle rate converge in finite time.

If the above problems are solved, the high manoeuvering target will be intercepted more accurately in three-dimensional space. The main contributions and innovations of the guidance law proposed in this paper are summarised as follows:

(1) In the guidance law proposed in this paper, non-singular terminal sliding surface is designed and a fast power reaching law is selected. This allows the line-of-sight angle and line-of-sight angle rate to converge in finite time. At the same time, the chattering phenomenon of sliding mode control is eliminated.

(2) A new global RBF neural network is proposed to accurately estimate the perturbation of the guidance system caused by target manoeuvering. Compared with Refs [14, 39, 40], this method can realise the estimation and compensation of target manoeuvering without knowing the upper bound of target manoeuvering. In order to improve the estimation accuracy and accelerate the convergence characteristics of RBF neural network, the parameters of RBF neural network are adjusted online in real time.

(3) An adaptive law is designed to compensate the estimation error of RBF neural network and improve the convergence speed of the guidance system. This allows the missile without a significant advantage in overload capability to successfully intercept more than 20g large manoeuvering targets with higher accuracy.

Moreover, literature [41] also uses the RBF neural network disturbance observer and non-singular terminal sliding mode control to design a guidance law. However, it differs from the guidance law proposed in this article in the following aspects:

(a) The non-singular terminal sliding mode surface is different. The non-singular terminal sliding mode surface proposed in this paper adopts a segmented design idea and has higher convergence accuracy.

(b) RBF neural network adaptive parameter design methods are different, this paper can make RBF neural network parameters adaptive adjustment to the optimal, and use the adaptive law to further eliminate the neural network disturbance estimation error. Therefore, the disturbance estimation accuracy is higher than that of the method in Ref. [41].

(c) The guidance law proposed in this paper is based on three-dimensional space, while that of in Ref. [41] only considers the two-dimensional plane.

The remainder of this article is organised as follows. In Section 2, equations of guidance system for the missile intercepting the target is presented in three-dimensional space. In Section 3, a new three-dimensional finite-time guidance law based on sliding mode adaptive RBF neural network is proposed for highly manoeuvering targets, and the finite-time convergence and stability are proved. In Section 4, the numerical simulation results are carried out under different kinds of scenarios of missile intercepting highly manoeuvering targets to demonstrate and evaluate the effectiveness and superiority of the proposed guidance law. In Section 5, the crucial conclusion of the whole paper is presented.
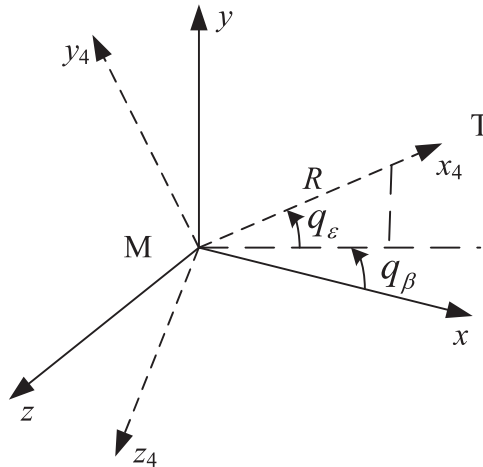
Figure 1. *Three-dimensional relative motion of a missile to a target.*

2.0 Formulation of guidance mode

This article only models the navigation system. In the establishment of guidance model, we regard the missile as a mass point, without considering its aerodynamic characteristics, mass characteristics, inertia characteristics as well as propulsion characteristics, and without limiting its flight envelope. It assumes that the available overload of the missile flight control system is 40g.

This section demonstrates equations of guidance system for the missile intercepting the target. In order to be more practical and reduce the influence of coupling between channels, the three-dimensional guidance model is considered. Figure 1 shows the three-dimensional relative motion of a missile to a target. In the guidance model, the missile and the target are treated as particles. The missile is denoted by M and the target is denoted by T. $Mxyz$ is an inertial coordinate system. $Mx_4y_4z_4$ is a line-of-sight coordinate system. The relative distance between the missile and the target is denoted by R. The elevation and azimuth angles of the line-of-sight are denoted by q_ε and q_β, respectively. The vectors of the missile's acceleration and target's acceleration are denoted by $a_M = [\, a_{MR} \; a_{M\varepsilon} \; a_{M\beta} \,]^T$ and $a_T = [\, a_{TR} \; a_{T\varepsilon} \; a_{T\beta} \,]^T$ in the line-of-sight coordinate system separately.

The relative motion equation of a missile to a target can be obtained from Fig. 1. Let the rotational angular velocity of the line-of-sight coordinate system relative to the ground inertial coordinate system be ω. The relative velocity vector is expressed in Equation (1).

$$V(R, q_\varepsilon, q_\beta) = \begin{bmatrix} \dot{R} \\ R\dot{q}_\varepsilon \\ -R\dot{q}_\beta \cos q_\varepsilon \end{bmatrix} \tag{1}$$

According to the solution method of vector derivative, Equation (2) can be obtained.

$$\frac{dV}{dt} = \omega \times V + \frac{\partial V}{\partial t} = a_T - a_M \tag{2}$$

In Equation (2), dV/dt is the derivative of the relative velocity with respecting to time in inertial coordinates. $\partial V/\partial t$ is the derivative of the relative velocity with respecting to time in the line-of-sight coordinate system. $\omega \times$ is given by Equation (3).

$$\omega \times = \begin{bmatrix} 0 & -\dot{q}_\varepsilon & \dot{q}_\beta \cos q_\varepsilon \\ \dot{q}_\varepsilon & 0 & -\dot{q}_\beta \sin q_\varepsilon \\ -\dot{q}_\beta \cos q_\varepsilon & \dot{q}_\beta \sin q_\varepsilon & 0 \end{bmatrix} \tag{3}$$

Substituting Equations (1) and (3) into Equation (2), we can get Equation (4).

$$\begin{bmatrix} 0 & -\dot{q}_\varepsilon & \dot{q}_\beta \cos q_\varepsilon \\ \dot{q}_\varepsilon & 0 & -\dot{q}_\beta \sin q_\varepsilon \\ -\dot{q}_\beta \cos q_\varepsilon & \dot{q}_\beta \sin q_\varepsilon & 0 \end{bmatrix} \begin{bmatrix} \dot{R} \\ R\dot{q}_\varepsilon \\ -R\dot{q}_\beta \cos q_\varepsilon \end{bmatrix} +$$
$$\begin{bmatrix} \ddot{R} \\ R\ddot{q}_\varepsilon + \dot{R}\dot{q}_\varepsilon \\ -R\ddot{q}_\beta \cos q_\varepsilon - \dot{R}\dot{q}_\beta \cos q_\varepsilon + R\dot{q}_\varepsilon \dot{q}_\beta \sin q_\varepsilon \end{bmatrix} = a_T - a_M \tag{4}$$

Expanding Equation (4) produces Equation (5).

$$\begin{cases} \ddot{R} - R\dot{q}_\varepsilon^2 - R\dot{q}_\beta^2 \cos^2 q_\varepsilon = a_{TR} - a_{MR} \\ R\ddot{q}_\varepsilon + 2\dot{R}\dot{q}_\varepsilon + R\dot{q}_\beta^2 \sin q_\varepsilon \cos q_\varepsilon = a_{T\varepsilon} - a_{M\varepsilon} \\ -R\ddot{q}_\beta \cos q_\varepsilon - 2\dot{R}\dot{q}_\beta \cos q_\varepsilon + 2R\dot{q}_\varepsilon \dot{q}_\beta \sin q_\varepsilon = a_{T\beta} - a_{M\beta} \end{cases} \tag{5}$$

From Equation (5), we can solve for $\ddot{q}_\varepsilon$ and $\ddot{q}_\beta$, given by Equation (6).

$$\begin{cases} \ddot{q}_\varepsilon = -\dfrac{2\dot{R}}{R}\dot{q}_\varepsilon - \dot{q}_\beta^2 \sin q_\varepsilon \cos q_\varepsilon - \dfrac{a_{M\varepsilon}}{R} + \dfrac{a_{T\varepsilon}}{R} \\ \ddot{q}_\beta = -\dfrac{2\dot{R}}{R}\dot{q}_\beta + 2\dot{q}_\varepsilon \dot{q}_\beta \tan q_\varepsilon + \dfrac{a_{M\beta}}{R \cos q_\varepsilon} - \dfrac{a_{T\beta}}{R \cos q_\varepsilon} \end{cases} \tag{6}$$

According to Ref. [20], the problem of missile collision angle constraint is equivalent to that of line-of-sight angle tracking. The desired terminal line-of-sight angles are defined as $q_{\varepsilon d}$ and $q_{\beta d}$. let $x_1 = q_\varepsilon - q_{\varepsilon d}$, $x_2 = q_\beta - q_{\beta d}$, $x_3 = \dot{q}_\varepsilon$, $x_4 = \dot{q}_\beta$. The guidance system state equation in three-dimensional space can be demonstrated by Equation (7).

$$\begin{cases} \dot{x}_1 = x_3 \\ \dot{x}_2 = x_4 \\ \dot{x}_3 = -\dfrac{2\dot{R}}{R}x_3 - x_4^2 \sin q_\varepsilon \cos q_\varepsilon - \dfrac{a_{M\varepsilon}}{R} + d_\varepsilon \\ \dot{x}_4 = -\dfrac{2\dot{R}}{R}x_4 + 2x_3 x_4 \tan q_\varepsilon + \dfrac{a_{M\beta}}{R \cos q_\varepsilon} + d_\beta \end{cases} \tag{7}$$

In Equation (7), d_ε and d_β are the disturbance caused by the manoeuvering information of the target. The expressions of d_ε and d_β are respectively demonstrated by Equation (8).

$$\begin{cases} d_\varepsilon = \dfrac{a_{T\varepsilon}}{R} \\ d_\beta = -\dfrac{a_{T\beta}}{R \cos q_\varepsilon} \end{cases} \tag{8}$$

Equation (7) can be further simplified into Equation (9). The expressions of f_1, f_2 and b_1, b_2 are respectively demonstrated by Equations (10) and (11).

$$\begin{cases} \dot{x}_1 = x_3 \\ \dot{x}_2 = x_4 \\ \dot{x}_3 = f_1 + b_1 a_{M\varepsilon} + d_\varepsilon \\ \dot{x}_4 = f_2 + b_2 a_{M\beta} + d_\beta \end{cases} \tag{9}$$

$$\begin{cases} f_1 = -\dfrac{2\dot{R}}{R}x_3 - x_4^2 \sin q_\varepsilon \cos q_\varepsilon \\ f_2 = -\dfrac{2\dot{R}}{R}x_4 + 2x_3 x_4 \tan q_\varepsilon \end{cases} \tag{10}$$

$$\begin{cases} b_1 = -\dfrac{1}{R} \\ b_2 = \dfrac{1}{R\cos q_\varepsilon} \end{cases} \tag{11}$$

3.0 The design of guidance law

In this section, a new three-dimensional finite-time convergence guidance law is developed, based on sliding mode adaptive RBF neural network against highly manoeuvering targets. By using the Lyapunov stability theory, the finite-time convergence and stability are analysed, and the optimal adaptive parameters are designed.

The guidance system Equation (9) can be rewritten as Equation (12)–(14).

$$x = \begin{bmatrix} x_1 \\ x_2 \end{bmatrix} = \begin{bmatrix} q_\varepsilon - q_{\varepsilon d} \\ q_\beta - q_{\beta d} \end{bmatrix} \tag{12}$$

$$\dot{x} = \begin{bmatrix} \dot{x}_1 \\ \dot{x}_2 \end{bmatrix} = \begin{bmatrix} x_3 \\ x_4 \end{bmatrix} = \begin{bmatrix} \dot{q}_\varepsilon \\ \dot{q}_\beta \end{bmatrix} \tag{13}$$

$$\ddot{x} = \begin{bmatrix} \dot{x}_3 \\ \dot{x}_4 \end{bmatrix} = f + Bu + d \tag{14}$$

where

$$f = \begin{bmatrix} f_1 \\ f_2 \end{bmatrix} = \begin{bmatrix} -\dfrac{2\dot{R}}{R}x_3 - x_4{}^2 \sin q_\varepsilon \cos q_\varepsilon \\ -\dfrac{2\dot{R}}{R}x_4 + 2x_3 x_4 \tan q_\varepsilon \end{bmatrix} \tag{15}$$

$$B = \begin{bmatrix} b_1 & 0 \\ 0 & b_2 \end{bmatrix} = \begin{bmatrix} -\dfrac{1}{R} & 0 \\ 0 & \dfrac{1}{R\cos q_\varepsilon} \end{bmatrix} \tag{16}$$

$$d = \begin{bmatrix} d_1 \\ d_2 \end{bmatrix} = \begin{bmatrix} d_\varepsilon \\ d_\beta \end{bmatrix} = \begin{bmatrix} \dfrac{a_{T\varepsilon}}{R} \\ -\dfrac{a_{T\beta}}{R\cos q_\varepsilon} \end{bmatrix} \tag{17}$$

$$u = \begin{bmatrix} u_1 \\ u_2 \end{bmatrix} = \begin{bmatrix} u_\varepsilon \\ u_\beta \end{bmatrix} = \begin{bmatrix} a_{M\varepsilon} \\ a_{M\beta} \end{bmatrix} \tag{18}$$

3.1 Guidance law design and its stability analysis

In order to cancel the line-of-sight angle error and allow the line-of-sight angle rate to converge quickly to zero, an appropriate non-singular terminal sliding surface is designed. The specific form is as follows:

$$s = \begin{bmatrix} s_1 \\ s_2 \end{bmatrix} = \begin{bmatrix} \dot{x}_1 + \alpha_1 x_1 + \alpha_2 g(x_1) \\ \dot{x}_2 + \alpha_1 x_2 + \alpha_2 g(x_2) \end{bmatrix} = \dot{x} + \alpha_1 x + \alpha_2 g(x) \tag{19}$$

where $\alpha_1 > 0, \alpha_2 > 0$ and $g(x) \in R$ is defined as follows:

$$g(x) = \begin{bmatrix} g(x_1) \\ g(x_2) \end{bmatrix} \tag{20}$$

$$g(x_i) = \begin{cases} \mathrm{sig}(x_i)^\lambda, & |x_i| > \eta \\ \gamma_1 x_i + \gamma_2 \mathrm{sign}(x_i)x_i^2, & |x_i| \le \eta \end{cases} \quad i = 1, 2 \tag{21}$$

$$\gamma_1 = (2 - \gamma)\eta^{\lambda - 1} \tag{22}$$

$$\gamma_2 = (\gamma - 1)\eta^{\lambda - 2} \tag{23}$$

where $0 < \lambda < 1$, $0 < \gamma < 1$ and η is a small positive constant. $sig(x_i)^\lambda = |x_i|^\lambda sgn(x_i)$.

Remark 1. The sliding surface proposed in this paper can ensure that the sliding manifolds converge to a small area instead of zero within a finite time, avoiding the system chattering phenomenon caused by crossing the sliding surface, and at the same time, ensure that the system state converges to a small area in a finite time. The following Theorem 1 reveals a detailed explanation.

The derivative of s is expressed as follows.

$$\dot{s} = \begin{bmatrix} \dot{s}_1 \\ \dot{s}_2 \end{bmatrix} = \ddot{x} + \alpha_1 \dot{x} + \alpha_2 \dot{g}(x) = f + Bu + d + l \tag{24}$$

where

$$l = \alpha_1 \dot{x} + \alpha_2 \dot{g}(x) \tag{25}$$

$$\dot{g}(x) = \begin{bmatrix} \dot{g}(x_1) \\ \dot{g}(x_2) \end{bmatrix} \tag{26}$$

$$\dot{g}(x_i) = \begin{cases} \lambda |x_i|^{\lambda - 1} \dot{x}_i, & |x_i| > \eta \\ \gamma_1 \dot{x}_i + 2\gamma_2 x_i \dot{x}_i sign(x_i), & |x_i| \le \eta \end{cases} \quad i = 1, 2 \tag{27}$$

In order to make the system state trajectory converge rapidly from the initial state to the designed sliding mode surfaces, a fast power reaching law is selected as follows:

$$\dot{s} = \begin{bmatrix} \dot{s}_1 \\ \dot{s}_2 \end{bmatrix} = -k_2 s - k_1 sig(s)^\gamma = \begin{bmatrix} -k_2 s_1 - k_1 sig(s_1)^\gamma \\ -k_2 s_2 - k_1 sig(s_2)^\gamma \end{bmatrix} \tag{28}$$

where $k_1 > 0, k_2 > 0$.

Then design the guidance law as follows:

$$u = -B^{-1}(f + \hat{d} + ad + l + k_2 s + k_1 sig(s)^\gamma) \tag{29}$$

where $\hat{d}$ shown as Equation (30) is the estimation term of the system disturbance d caused by the target manoeuvering. ad is an adaptive term in order to eliminate the influence of system disturbance estimation error on the guidance system and improve the convergence speed of the guidance system. The expression of the adaptive term ad is designed as Equation (31). In this equation, the first term is used to accelerate the convergence rate of the guidance system and the second term is used to reduce the impact of the system disturbance estimation error.

$$\hat{d} = \begin{bmatrix} \hat{d}_1 \\ \hat{d}_2 \end{bmatrix} \tag{30}$$

$$ad = \begin{bmatrix} ad_1 \\ ad_2 \end{bmatrix} = \begin{bmatrix} \dfrac{s_1}{|s_1| + \mu}\hat{\chi}_1 + \hat{\delta}_1 \\ \dfrac{s_2}{|s_2| + \mu}\hat{\chi}_2 + \hat{\delta}_2 \end{bmatrix} \tag{31}$$

where

$$\dot{\hat{\delta}}_i = \eta_1 s_i, i = 1, 2 \tag{32}$$

$$\dot{\hat{\chi}}_i = \frac{s_i^2}{|s_i| + \mu}, i = 1, 2 \tag{33}$$

$$\tilde{\chi}_i = \hat{\chi}_i - \chi_i, i = 1, 2 \tag{34}$$

Next, the stability and finite time convergence of the guidance system will be analysed and proved. Before that, the following lemma is introduced.

Lemma 1. *[39] For the nonlinear system $\dot{x} = f(x, t), x \in R^n$, it can assume that there exists a positive definite and continuous function $V(x)$. The derivative of $V(x)$ satisfies inequality (35)*

$$\dot{V}(x) \le -\mu V(x) - \lambda V^\alpha(x) \tag{35}$$

where $\mu > 0$, $\lambda > 0$ and $0 < \alpha < 1$, if the initial time is t_0 and $x(t_0) = x_0$, the time from the initial state to the equilibrium point of the system satisfies the following inequality:

$$\mathrm{T} \le \frac{1}{\mu(1 - \alpha)} \ln \frac{\mu V^{1-\alpha}(x_0) + \lambda}{\lambda} \tag{36}$$

This inequality indicates that the system states converge in a finite-time.

Theorem 1. *For the guidance system (14), the sliding mode surface is given as Equation (19), the reaching law is given as Equation (28) and the guidance law is given as Equation (29). We can achieve the following conclusions.*

(a) *In a finite-time, the sliding manifold s is converged to the small region $|\mathrm{s}| \le \varepsilon_1$, where ε_1 is a very small positive constant.*

(b) *In a finite-time, the line-of-sight angle errors $q_\varepsilon - q_{\varepsilon d}$ and $q_\beta - q_{\beta d}$ are converged to the small regions $|q_\varepsilon - q_{\varepsilon d}| < \eta$ and $|q_\beta - q_{\beta d}| < \eta$, where η is a very small positive constant.*

(c) *In a finite-time, the line-of-sight angle rate $\dot{q}_\varepsilon$ and $\dot{q}_\beta$ are converged to the small regions $|\dot{q}_\varepsilon| < \eta\eta$ and $|\dot{q}_\beta| < \eta\eta$, where*

$$\eta\eta = \alpha_1 \eta + \alpha_2 \eta^\lambda + \varepsilon_1 \tag{37}$$

Proof. A Lyapunov function V_1 is selected as Equation (38).

$$V_1 = \frac{1}{2} s^T s \tag{38}$$

The residual estimation error of the guidance system disturbance is expressed as follows:

$$\left| d - \hat{d} - ad \right| \le \varepsilon \tag{39}$$

The derivative of V_1 is expressed as follows.

$$\begin{aligned}
\dot{V}_1 &= s^T \dot{s} \\
&= s^T(f + Bu + d + l) \\
&= s^T(d - \hat{d} - ad - k_2 s - k_1 \mathrm{sig}(s)^\gamma) \\
&\le -k_2|s|^2 - k_1|s|^{\gamma+1} + \varepsilon |s|
\end{aligned} \tag{40}$$

Rewrite the formula (40) into the following two forms:

$$\dot{V}_1 \le -k_2|s|^2 - (k_1|s|^\gamma - \varepsilon) |s| \tag{41}$$

$$\dot{V}_1 \le -(k_2 |s| - \varepsilon) |s| - k_1|s|^{\gamma+1} \tag{42}$$

When $k_1|s|^\gamma - \varepsilon \ge 0$, $|\mathrm{s}| \ge (\varepsilon/k_1)^{1/\gamma}$,

$$\dot{V}_1 \le -k_2|s|^2 = -2k_2 V_1 \tag{43}$$

When $k_2 |s| - \varepsilon \ge 0$, $|\mathrm{s}| \ge (\varepsilon/k_2)$,

$$\dot{V}_1 \le -k_1|s|^{\gamma+1} = -2^{\frac{\gamma+1}{2}} k_1 V_1^{\frac{\gamma+1}{2}} \tag{44}$$

It can be known from Lemma 1 and the inequality (43) and (44) that the sliding manifold s is converged to the small region $|s| \le \min\left\{(\varepsilon/k_1)^{1/\gamma}, (\varepsilon/k_2)\right\} = \varepsilon_1$ within a finite-time. where ε_1 is a very small positive constant. Therefore, conclusion (a) is proved.

Case 1. *If* $|x_i| \ge \eta, i = 1, 2$, A Lyapunov function V_2 is selected as Equation (45).

$$V_2 = \frac{1}{2}x_i x_i, i = 1, 2 \tag{45}$$

When $|s| \le \min\left\{(\varepsilon/k_1)^{1/\gamma}, (\varepsilon/k_2)\right\} = \varepsilon_1$, according to Equation (19), the inequality (46) can be obtained.

$$\dot{x}_i \le -\alpha_1 x_i - \alpha_2 \text{sig}(x_i)^\lambda + \varepsilon_1 \tag{46}$$

The derivation of V_2 is expressed as the inequality (47).

$$\begin{aligned} \dot{V}_2 &= x_i \dot{x}_i \\ &\le -x_i(\alpha_1 x_i + \alpha_2 \text{sig}(x_i)^\lambda - \varepsilon_1) \\ &\le -\alpha_1 |x_i|^2 - \alpha_2 |x_i|^{\lambda+1} + \varepsilon_1 |x_i| \end{aligned} \tag{47}$$

Rewrite the inequality (47) in the following two forms:

$$\dot{V}_2 \le -\alpha_1 |x_i|^2 - (\alpha_2 |x_i|^\lambda - \varepsilon_1) |x_i| \tag{48}$$

$$\dot{V}_2 \le -(\alpha_1 |x_i| - \varepsilon_1) |x_i| - \alpha_2 |x_i|^{\lambda+1} \tag{49}$$

When $\alpha_2 |x_i|^\lambda - \varepsilon_1 \ge 0$, $|x_i| \ge (\varepsilon_1/\alpha_2)^{1/\lambda}$,

$$\dot{V}_2 \le -\alpha_1 |x_i|^2 = -2\alpha_1 V_2 \tag{50}$$

When $\alpha_1 |x_i| - \varepsilon_1 \ge 0$, $|x_i| \ge (\varepsilon_1/\alpha_1)$,

$$\dot{V}_2 \le -\alpha_2 |x_i|^{\lambda+1} = -2^{\frac{\lambda+1}{2}}\alpha_2 V_2^{\frac{\lambda+1}{2}} \tag{51}$$

Supposed that $\min\left\{(\varepsilon_1/\alpha_2)^{1/\lambda}, (\varepsilon_1/\alpha_1)\right\} \le \eta$, it can be known from Lemma 1 and the inequality (50) and (51) that x_i is converged to the very small region $|x_i| < \eta, i = 1, 2$ within a finite-time. So the line-of-sight angle errors $q_\varepsilon - q_{\varepsilon d}$ and $q_\beta - q_{\beta d}$ are converged to the small regions $|q_\varepsilon - q_{\varepsilon d}| < \eta$ and $|q_\beta - q_{\beta d}| < \eta$ within a finite-time. Conclusion (b) is proved.

Case 2. If $|x_i| < \eta, i = 1, 2$, when $|s| \le \min\left\{(\varepsilon/k_1)^{1/\gamma}, (\varepsilon/k_2)\right\} = \varepsilon_1$, according to Equation (19), the inequality (52) and (53) can be easily obtained.

$$\dot{x}_i \le -\alpha_1 x_i - \alpha_2(\gamma_1 x_i + \gamma_2 sign(x_i)x_i^2) + \varepsilon_1 \tag{52}$$

$$\begin{aligned} |\dot{x}_i| &\le \left|\alpha_1 x_i + \alpha_2(\gamma_1 x_i + \gamma_2 sign(x_i)x_i^2)\right| + \varepsilon_1 \\ &\le |\alpha_1 x_i| + \left|\alpha_2(\gamma_1 x_i + \gamma_2 sign(x_i)x_i^2)\right| + \varepsilon_1 \\ &\le \alpha_1 \eta + \alpha_2 \eta^\lambda + \varepsilon_1 = \eta\eta \end{aligned} \tag{53}$$

Then, $\dot{x}_i$ is converged to the very small region $|\dot{x}_i| < \eta\eta, i = 1, 2$ within a finite-time. So the line-of-sight angle rate $\dot{q}_\varepsilon$ and $\dot{q}_\beta$ are converged to the small regions $|\dot{q}_\varepsilon| < \eta\eta$ and $|\dot{q}_\beta| < \eta\eta$ within a finite-time. Conclusion (c) is proved.

3.2 RBF neural network disturbance observer design

In order to intercept large manoeuvering targets accurately, it is necessary to estimate the disturbance of the guidance system caused by target manoeuvering. In this paper, a new global RBF neural network is proposed to estimate the disturbance. The disturbance $d = \begin{bmatrix} d_1 & d_2 \end{bmatrix}^T$ can be estimated using the RBF neural network as Equation (54).

$$d_i = \sum_{j=1}^{m} w_{ij}^* h_{ij}^* + \varepsilon_{i0} = W_i^{*T} h_i^* + \varepsilon_{i0} = d_i^* + \varepsilon_{i0}, i = 1, 2 \tag{54}$$

Where $W_i^* = \begin{bmatrix} w_{i1}^* w_{i2}^* \ldots w_{im}^* \end{bmatrix}^T, i = 1, 2$ are optimal output weight vectors of the output layer of the RBF neural network. $\varepsilon_{i0}, i = 1, 2$ are the optimal estimation error. $d_i^*, i = 1, 2$ are the optimal approximation of the disturbance $d_i, i = 1, 2$. $h_i^* = \begin{bmatrix} h_{i1}^* h_{i2}^* \ldots h_{im}^* \end{bmatrix}^T, i = 1, 2$ are optimal vectors whose elements are given by Equation (55) which represents the Gaussian activation function of RBF neural network hidden layer neurons.

$$h_{ij}^* = \exp\left(\frac{-\|x - c_{ij}^*\|^2}{2\sigma_{ij}^{*2}}\right), i = 1, 2 \tag{55}$$

Where c_{ij}^* is the optimal centre and σ_{ij}^* is the optimal width for the j_{th} Gaussian function.
The RBF neural network disturbance estimator is chosen as Equation (56).

$$\hat{d}_i = \sum_{j=1}^{m} \hat{w}_{ij} \hat{h}_{ij} = \hat{W}_i^T \hat{h}_i, i = 1, 2, j = 1, 2, 3 \cdots m \tag{56}$$

Where $\hat{W}_i = \begin{bmatrix} \hat{w}_{i1} \hat{w}_{i2} \ldots \hat{w}_{im} \end{bmatrix}^T, i = 1, 2$ that adaptively adjust online are output weight vector of the RBF neural network linear output layer. $\hat{h}_i = \begin{bmatrix} \hat{h}_{i1} \hat{h}_{i2} \ldots \hat{h}_{im} \end{bmatrix}^T, i = 1, 2$ that also adaptively adjusts online are the activation function vectors of the hidden layer neurons of the RBF neural network. The elements of $\hat{h}_i$ are given by Equation (57).

$$\hat{h}_{ij} = \exp\left(\frac{-\|x - \hat{c}_{ij}\|^2}{2\hat{\sigma}_{ij}^2}\right), i = 1, 2, j = 1, 2, 3 \cdots m \tag{57}$$

Let the optimal approximation of the disturbance $d_i^*, i = 1, 2$ subtract the adaptive approximation of the disturbance $\hat{d}_i, i = 1, 2$. Then we use linearisation techniques to expand it into a partially linear form of Taylor expansion series. Equation (58) is obtained.

$$d_i^* - \hat{d}_i = W_i^{*T} h_i^* - \hat{W}_i^T \hat{h}_i = -\tilde{W}_i^T \hat{h}_i - \hat{W}_i \frac{\partial h_i}{\partial c_i} \tilde{c}_i - \hat{W}_i \frac{\partial h_i}{\partial \sigma_i} \tilde{\sigma}_i + \varepsilon_{i1}, i = 1, 2 \tag{58}$$

Where $\tilde{W}_i = \hat{W}_i - W_i^*, i = 1, 2$ are the deviation of weight vectors between the adaptive weight vectors $\hat{W}_i$ and the optimal weight vectors W_i^* for the linear output layer of RBF neural network. $\tilde{c}_i = \hat{c}_i - c_i^*, i = 1, 2$ are the deviation centre vectors of the Gaussian function between the adaptive centre vectors $\hat{c}_i$ and the optimal centre vectors c_i^*. $\tilde{\sigma}_i = \hat{\sigma}_i - \sigma_i^*, i = 1, 2$ are the deviation of the width vectors between the adaptive width vectors $\hat{\sigma}_i$ and the optimal width vectors σ_i^*. $\varepsilon_{i1}, i = 1, 2$ are the error for the Taylor series. $\frac{\partial h_i}{\partial c_i}, i = 1, 2$ are given by Equation (59) and $\frac{\partial h_i}{\partial \sigma_i}, i = 1, 2$ are given by Equation (60), respectively.

$$\frac{\partial h_i}{\partial c_i} = h'_{ci} = \begin{bmatrix} \frac{\partial h_{i1}}{\partial c_{i1}} & 0 & 0 & 0 \\ 0 & \frac{\partial h_{i2}}{\partial c_{i2}} & 0 & 0 \\ \ldots & \ldots & \ldots & \ldots \\ \ldots & \ldots & \ldots & \frac{\partial h_{im}}{\partial c_{im}} \end{bmatrix} \in R^{m \times m}, i = 1, 2 \tag{59}$$

$$\frac{\partial h_i}{\partial \sigma_i} = h'_{\sigma i} = \begin{bmatrix} \frac{\partial h_{i1}}{\partial \sigma_{i1}} & 0 & 0 & 0 \\ 0 & \frac{\partial h_{i2}}{\partial \sigma_{i2}} & 0 & 0 \\ \ldots & \ldots & \ldots & \ldots \\ \ldots & \ldots & \ldots & \frac{\partial h_{im}}{\partial \sigma_{im}} \end{bmatrix} \in R^{m \times m}, i = 1, 2 \tag{60}$$

Substituting Equation (29) into Equation (24), Equation (61) can be obtained.

$$\dot{s}_i = d_i - \hat{d}_i - ad_i - k_2 s_i - k_1 \text{sig}(s_i)^\gamma, i = 1, 2 \tag{61}$$

Substituting Equations (31) and (58) into Equation (61), Equation (62) can be obtained.

$$\dot{s}_i = -\tilde{W}_i^T \hat{h}_i - \hat{W}_i h_{\sigma i} \tilde{c}_i - \hat{W}_i h'_{\sigma i} \tilde{\sigma}_i + \delta_i \\ -\frac{s_i}{|s_i| + \mu} \hat{\chi}_i - \hat{\delta}_i - k_2 s_i - k_1 \text{sig}(s_i)^\gamma, i = 1, 2 \tag{62}$$

Where $\delta_i = \varepsilon_{0i} + \varepsilon_{1i}$, $i = 1, 2$ are total RBF neural network estimation error for the system disturbance. It is the sum of the optimal estimation error (ε_{i0}, $i = 1, 2$) and the error for the Taylor series (ε_{i1}, $i = 1, 2$).

Define $\tilde{\delta}_i$, $i = 1, 2$ to be the deviation of the total RBF neural network estimation error for the system disturbance between the adaptive estimation error $\hat{\delta}_i$ and the actual estimation error δ_i, which is expressed by Equation (63).

$$\tilde{\delta}_i = \hat{\delta}_i - \delta_i, i = 1, 2 \tag{63}$$

Substituting Equation (63) into Equation (62), Equation (64) can be obtained.

$$\dot{s}_i = -\tilde{W}_i^T \hat{h}_i - \hat{W}_i h'_{ci} \tilde{c}_i - \hat{W}_i h'_{\sigma i} \tilde{\sigma}_i - \tilde{\delta}_i - \frac{s_i}{|s_i| + \mu} \hat{\chi}_i - k_2 s_i - k_1 \mathrm{sig}(s_i)^\gamma, i = 1, 2 \tag{64}$$

In order to prove the stability of the guidance system expressed in Equation (14) under the guidance law expressed in Equation (29), the Lyapunov function is selected in Equation (65).

$$V_{0i} = \frac{1}{2}s_i^2 + \frac{1}{2}\tilde{\chi}_i^2 + \frac{1}{2\eta_1}\tilde{\delta}_i^2 + \frac{1}{2\eta_2}\tilde{W}_i^T \tilde{W}_i + \frac{1}{2\eta_3}\tilde{c}_i^T \tilde{c}_i + \frac{1}{2\eta_4}\tilde{\sigma}_i^T \tilde{\sigma}_i, i = 1, 2 \tag{65}$$

Where η_1, η_2, η_3 and η_4 are designed parameters, $\tilde{\chi}_i = \hat{\chi}_i - \chi_i$, $i = 1, 2$ are the error between the adaptive gain $\hat{\chi}_i$ and the fixed gain χ_i.

Take the derivative of the Lyapunov function and get Equation (66).

$$\dot{V}_{0i} = s_i \dot{s}_i + \tilde{\chi}_i \dot{\tilde{\chi}}_i + \frac{1}{\eta_1}\tilde{\delta}_i \dot{\tilde{\delta}}_i + \frac{1}{\eta_2}\tilde{W}_i^T \dot{\tilde{W}}_i + \frac{1}{\eta_3}\tilde{c}_i^T \dot{\tilde{c}}_i + \frac{1}{\eta_4}\tilde{\sigma}_i^T \dot{\tilde{\sigma}}_i, i = 1, 2 \tag{66}$$

Substituting in Equation (64) into Equation (66), Equation (67) can be obtained.

$$\dot{V}_{0i} = s_i \left(-\tilde{W}_i^T \hat{h}_i - \hat{W}_i h'_{ci} \tilde{c}_i - \hat{W}_i h'_{\sigma i} \tilde{\sigma}_i - \tilde{\delta}_i - \frac{s_i}{|s_i| + \mu} \hat{\chi}_i - k_2 s_i - k_1 \mathrm{sig}(s_i)^\gamma \right)$$
$$+ \tilde{\chi}_i \dot{\tilde{\chi}}_i + \frac{1}{\eta_1}\tilde{\delta}_i \dot{\tilde{\delta}}_i + \frac{1}{\eta_2}\tilde{W}_i^T \dot{\tilde{W}}_i + \frac{1}{\eta_3}\tilde{c}_i^T \dot{\tilde{c}}_i + \frac{1}{\eta_4}\tilde{\sigma}_i^T \dot{\tilde{\sigma}}_i, i = 1, 2 \tag{67}$$

Substituting $\dot{\tilde{\delta}}_i = \dot{\hat{\delta}}_i, \dot{\tilde{\chi}}_i = \dot{\hat{\chi}}_i, \dot{\tilde{W}}_i = \dot{\hat{W}}_i$, $\dot{\tilde{c}}_i = \dot{\hat{c}}_i$ and $\dot{\tilde{\sigma}}_i = \dot{\hat{\sigma}}_i$ into Equation (67), Equation (68) can be obtained.

$$\dot{V}_{0i} = s_i \left(-\tilde{W}_i^T \hat{h}_i - \hat{W}_i h'_{ci} \tilde{c}_i - \hat{W}_i h'_{\sigma i} \tilde{\sigma}_i - \tilde{\delta}_i - \frac{s_i}{|s_i| + \mu} \hat{\chi}_i - k_2 s_i - k_1 \mathrm{sig}(s_i)^\gamma \right)$$
$$+ \tilde{\chi}_i \dot{\hat{\chi}}_i + \frac{1}{\eta_1}\tilde{\delta}_i \dot{\hat{\delta}}_i + \frac{1}{\eta_2}\tilde{W}_i^T \dot{\hat{W}}_i + \frac{1}{\eta_3}\tilde{c}_i^T \dot{\hat{c}}_i + \frac{1}{\eta_4}\tilde{\sigma}_i^T \dot{\hat{\sigma}}_i, i = 1, 2 \tag{68}$$

By rearranging and combining Equation (68), Equation (69) can be obtained.

$$\dot{V}_{0i} = s_i(-k_2 s_i - k_1 \mathrm{sig}(s_i)^\gamma) - \frac{s_i^2}{|s_i| + \mu}(\hat{\chi}_i - \tilde{\chi}_i) + \tilde{\delta}_i \left(\frac{1}{\eta_1}\dot{\hat{\delta}}_i - s_i \right) + \tilde{W}_i^T \left(\frac{1}{\eta_2}\dot{\hat{W}}_i - \hat{h}_i s_i \right)$$
$$+ \tilde{c}_i^T \left(\frac{1}{\eta_3}\dot{\hat{c}}_i - h'_{ci} s_i \hat{W}_i \right) + \tilde{\sigma}_i^T \left(\frac{1}{\eta_4}\dot{\hat{\sigma}}_i - h'_{\sigma i} s_i \hat{W}_i \right), i = 1, 2 \tag{69}$$

To guarantee that the guidance system expressed in Equation (14) under the guidance law expressed in Equation (29) is globally stable and the first derivative of the Lyapunov function $\dot{V}_{0i} < 0$ is satisfied, the time evolution of the adaptive estimation error $\hat{\delta}_i$, the adaptive weight vectors $\hat{W}_i$, the adaptive centre vectors $\hat{c}_i$ and the adaptive width vectors $\hat{\sigma}_i$ are chosen as Equation (70).

$$\dot{\hat{\delta}}_i = \eta_1 s_i, \dot{\hat{W}}_i = \eta_2 \hat{h}_i s_i, \dot{\hat{c}}_i = \eta_3 h'_{ci} s_i \hat{W}_i, \dot{\hat{\sigma}}_i = \eta_4 h'_{\sigma i} s_i \hat{W}_i, i = 1, 2 \tag{70}$$

Substituting Equations (34) and (70) into Equation (69), Equation (71) can be obtained.

$$\dot{V}_{0i} = s_i(-k_2 s_i - k_1 \mathrm{sig}(s_i)^\gamma) - \frac{s_i^2}{|s_i| + \mu}\chi_i, i = 1, 2 \tag{71}$$

According to Equation (71), the stability of the guidance system is guaranteed since the first derivative of the Lyapunov function $\dot{V}_{0i} < 0$ with the gain χ_i, $i = 1, 2$ as a positive value.

Table 1. *Initial condition of the missile and the target for the simulation*

Symbol	Symbol description	Value
$\theta_m(0)$	Initial elevation angle of the missile	15°
$\phi_m(0)$	Initial azimuth angle of the missile	0°
$[x_m(0), y_m(0), z_m(0)]$	Initial position of the missile	[0 0 0](km)
$v_m(0)$	Initial velocity of the missile	1,000m/s
$\theta_t(0)$	Initial elevation angle of the target	0°
$\phi_t(0)$	Initial azimuth angle of the target	0°
$[x_t(0), y_t(0), z_t(0)]$	Initial position of the target	[0,10,50] (km)
$v_t(0)$	Initial velocity of the target	−600m/s

Table 2. *Expected terminal line-of-sight angle*

Missile	$q_{\varepsilon d}(°)$	$q_{\beta d}(°)$
M1	30	−10
M2	20	0
M3	10	10
M4	0	20

The summary of the presented three-dimensional finite-time guidance law schemeis based on sliding mode adaptive RBF neural network against highly manoeuvering targets is as follows:

$$u = -B^{-1}(f + \hat{d} + ad + l + k_2 s + k_1 \text{sig}(s)^\gamma)$$

$$= \begin{bmatrix} u_1 \\ u_2 \end{bmatrix} = \begin{bmatrix} -\frac{1}{b_1}(f_1 + \hat{d}_1 + ad_1 + \alpha_1 \dot{x}_1 + \alpha_2 \dot{g}(x_1) + k_2 s_1 + k_1 \text{sig}(s_1)^\gamma) \\ -\frac{1}{b_2}(f_2 + \hat{d}_2 + ad_2 + \alpha_1 \dot{x}_2 + \alpha_2 \dot{g}(x_2) + k_2 s_2 + k_1 \text{sig}(s_2)^\gamma) \end{bmatrix}$$

$$= \begin{bmatrix} -\frac{1}{b_1}(-\frac{2\dot{R}}{R}x_3 - x_4{}^2 \sin q_\varepsilon \cos q_\varepsilon + \hat{W}_1^T \hat{h}_1 + \\ \frac{s_1}{|s_1| + \mu}\hat{\chi}_1 + \hat{\delta}_1 + \alpha_1 \dot{x}_1 + \alpha_2 \dot{g}(x_1) + k_2 s_1 + k_1 \text{sig}(s_1)^\gamma) \\ -\frac{1}{b_2}(-\frac{2\dot{R}}{R}x_4 + 2x_3 x_4 \tan q_\varepsilon + \hat{W}_2^T \hat{h}_2 + \\ \frac{s_2}{|s_2| + \mu}\hat{\chi}_2 + \hat{\delta}_2 + \alpha_1 \dot{x}_2 + \alpha_2 \dot{g}(x_2) + k_2 s_2 + k_1 \text{sig}(s_2)^\gamma) \end{bmatrix} \tag{72}$$

4.0 Simulation results

In this section, in order to demonstrate and evaluate the effectiveness and superiority of the proposed guidance law in Equation (72), the numerical simulation results are carried out under different kinds of scenarios of missile intercepting highly manoeuvering target. The simulation is divided into two parts. The first part, aiming at two different target manoeuver scenarios, verifies the effectiveness of the proposed guidance law at target interception accuracy and line-of-sight angle control accuracy. In the second part, in order to illustrate the superiority of the proposed guidance law, we compare it with other guidance laws in different manoeuver situations of the target.

In the following simulation, the guidance parameters of the guidance law designed in this paper are as follows:

$\alpha_1 = 10$, $\alpha_2 = 10$, $\lambda = 0.6$, $\eta = 0.01$, $\gamma = 0.9$, $k_1 = 6$, $k_2 = 2$, $\eta_1 = 1$, $\eta_2 = 15$, $\eta_3 = 15$, $\eta_4 = 1$, $\mu = 1$

The initial values of the integral variable parameters in the guidance law are as follows:

$\hat{\chi}_i(0) = 10$, $\hat{\delta}_i(0) = 0.001$, $\hat{W}_i(0) = [-60, -30, 0, 30, 60]$, $\hat{c}_i(0) = [-0.1, -0.05, 0, 0.05, 0.1]$, $\hat{\sigma}_i(0) = [3, 3, 3, 3, 3]$, $i = 1, 2$

It assume that the maximum available overload of the missile is 40g. Therefore, the guidance command is artificially limited to 40g in the simulation.
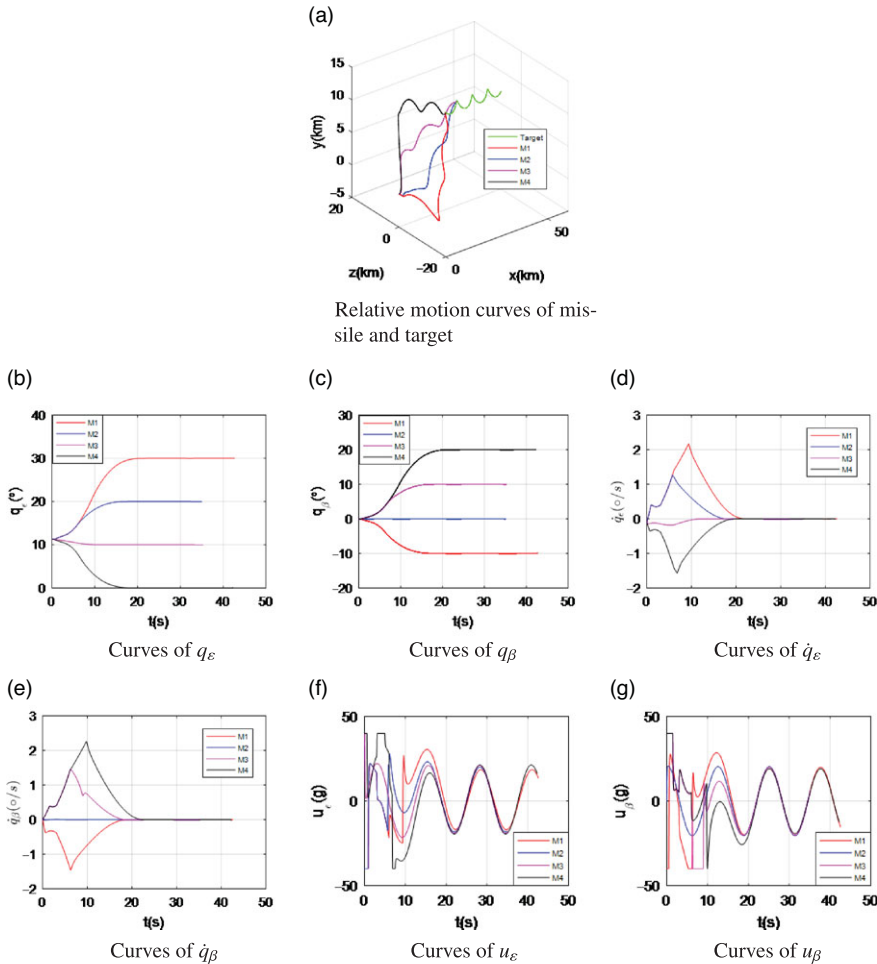
(a)

Relative motion curves of missile and target

(b)

Curves of q_ε

(c)

Curves of q_β

(d)

Curves of $\dot{q}_\varepsilon$

(e)

Curves of $\dot{q}_\beta$

(f)

Curves of u_ε

(g)

Curves of u_β

Figure 2. *Simulation results of four expected line-of-sight angles attack targets with Case 1.*

4.1 Effectiveness verification

To verify the effectiveness of the proposed guidance law, four missiles in the same initial position and state are considered to attack targets in two manoeuvering situations at their desired terminal line-of-sight angles. Initial conditions of the missile and the target for the simulation are shown as Table 1. The expected terminal line-of-sight angles of the four missiles attacking the target are shown in Table 2. Two different cases for target manoeuvers are as follows Case 1 and Case 2.

Case 1: $a_{T\varepsilon} = 200 \sin(0.5t)\text{m/s}^2$, $a_{T\beta} = 200 \cos(0.5t)\text{m/s}^2$.

Case 2: $a_{T\varepsilon} = -200\text{m/s}^2$, $a_{T\beta} = 200\text{m/s}^2$.

For Case 1, Fig. 2 and Table 3 show the simulation results of the proposed guidance law. The relative motion curves of the missile and the target are elaborated in Fig. 2(a). It can be known that four missiles with different expected terminal line-of-sight angles were all able to successfully intercept the target. The curves of q_ε and q_β for the four missiles are demonstrated in Fig. 2(b) and (c). It can be obtained that q_ε and q_β converge to different expected terminal line-of-sight angles precisely in a finite-time. The curves of $\dot{q}_\varepsilon$ and $\dot{q}_\beta$ for the four missiles are shown in Fig. 2(d) and (e). It is clearly revealed that the guidance system has the best convergence performance under the proposed guidance law in this paper. Figure 2(f)

Table 3. *Simulation results of four expected line-of-sight angles attack targets with Case 1*

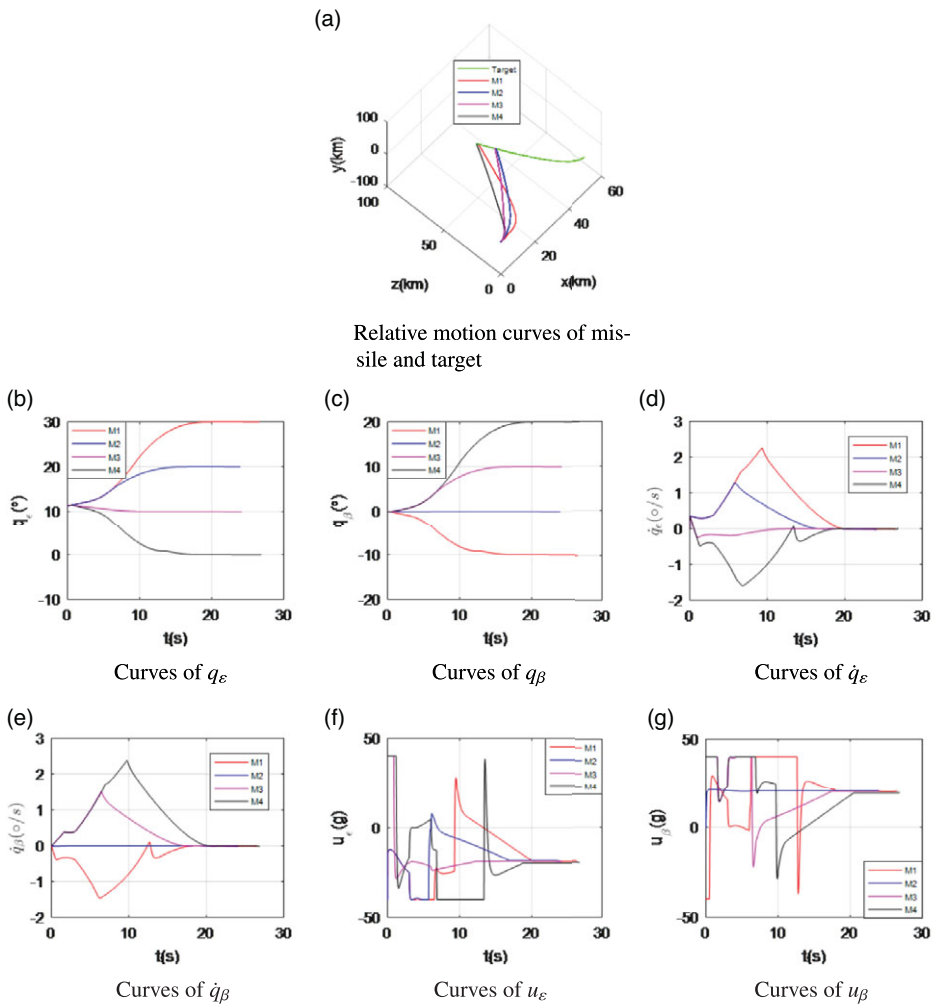| Missile	Miss distance(m)	Line-of-sight dip Angle error (°)	Line-of-sight drift Angle error (°)	Flight time(s)
M1	1.7258e-03	0.0052	0.0038	42.656
M2	1.4356e-03	0.0021	0.0013	34.954
M3	1.9507e-04	0.0018	0.0022	35.226
M4	8.3823e-05	0.0016	0.0026	42.247

(a)

Relative motion curves of missile and target

(b) Curves of q_ε

(c) Curves of q_β

(d) Curves of $\dot{q}_\varepsilon$

(e) Curves of $\dot{q}_\beta$

(f) Curves of u_ε

(g) Curves of u_β

Figure 3. *Simulation results of four expected line-of-sight angles attack targets with Case 2.*

and (g) indicate the curves of u_ε and u_β, which are within reasonable bounds. From Table 3, it can be known that all four missiles in the same initial state and at the same initial position under the proposed guidance law in this paper are able to accurately hit a manoeuvering target with the specified terminal line-of-sight angle. The maximum miss distance for the four missiles with different expected terminal sight angles is less than 0.002m, and the errors of the terminal line-of-sight angles are all controlled within 0.006°. The excellent control ability of the proposed guidance law in this paper to miss distance and expected terminal line-of-sight angle error is verified.

Table 4. *Simulation results of four expected line-of-sight angles attack targets with Case 2*

Missile	Miss distance(m)	Line-of-sight dip Angle error (°)	Line-of-sight drift Angle error (°)	Flight time(s)
M1	5.7938e-05	0.0057	0.0054	26.586
M2	2.1125e-05	0.0059	0.0067	23.936
M3	1.0087e-05	0.0066	0.0065	24.113
M4	1.3245e-05	0.0068	0.0058	26.859

For Case 2, when $a_{T\varepsilon} = -200\text{m/s}^2$, $a_{T\beta} = 200\text{m/s}^2$, Fig. 3 and Table 4 display the simulation results of the proposed guidance law. The relative motion curves of the missile and the target are revealed in Fig. 3(a). The curves of q_ε and q_β for the four missiles are manifested in Fig. 3(b) and (c). The curves of $\dot{q}_\varepsilon$ and $\dot{q}_\beta$ for the four missiles are shown in Fig. 3(d) and (e). The curves of u_ε and u_β for the four missiles are displayed in Fig. 3(f) and (g). Figure 3 shows the same situation as Fig. 2, so it will not be repeated here. From Table 4, it can be known that all four missiles in the same initial state and at the same initial position under the proposed guidance law in this paper are able to accurately hit a manoeuvering target with the specified terminal line-of-sight angle. The maximum miss distance for the four missiles with different expected terminal sight angles is less than 0.0001m, and the errors of the terminal line-of-sight angles are all controlled within 0.007°. The excellent control ability of the proposed guidance law in this paper to miss distance and expected terminal line-of-sight angle error is verified.

4.2 Superiority verification

To further verify the superiority of the proposed guidance law, the conventional proportional navigation guidance law and nonlinear terminal sliding mode guidance law [29] are selected for comparison. Initial conditions of the missile and the target for the simulation are shown as Table 1. Select the expected terminal line-of-sight angles $q_{\varepsilon d} = 30°$, $q_{\beta d} = 10°$. Two different cases for target manoeuvers are as follows Case 1 and Case 2.

Case 1: $a_{T\varepsilon} = 200 \sin(0.5t)\text{m/s}^2$, $a_{T\beta} = 200 \cos(0.5t)\text{m/s}^2$.

Case 2: $a_{T\varepsilon} = -200\text{m/s}^2$, $a_{T\beta} = 200\text{m/s}^2$.

The traditional proportional guidance law is shown as Equation (73).

$$u_{PNGL} = \begin{bmatrix} n_1 |\dot{R}| \dot{q}_\varepsilon \\ n_2 |\dot{R}| \dot{q}_\beta \end{bmatrix} \tag{73}$$

Where n_1 and n_2 are guidance parameters of the u_{PNGL}.

After a lot of simulations, the control effect of u_{PNGL} is optimised by adjusting the parameters. The final guidance parameters $n_1 = 4$ and $n_2 = 4$ are chosen.

The sliding surface of nonlinear terminal sliding mode guidance law (NTSMGL) is chosen as Equation (74).

$$s = \begin{bmatrix} s_1 \\ s_2 \end{bmatrix} = x + \frac{1}{\beta} \dot{x}^{p/q} \tag{74}$$

Where $\beta > 0$, p and q are positive odd numbers, and they satisfy $p > q$, $1 < p/q < 2$.

The NTSMGL is chosen as Equation (75).

$$u_{NTSMGL} = -B^{-1} \left(f + \frac{\beta q}{p} \dot{x}^{2-p/q} + ks + H\text{sgn}(s) \right) \tag{75}$$
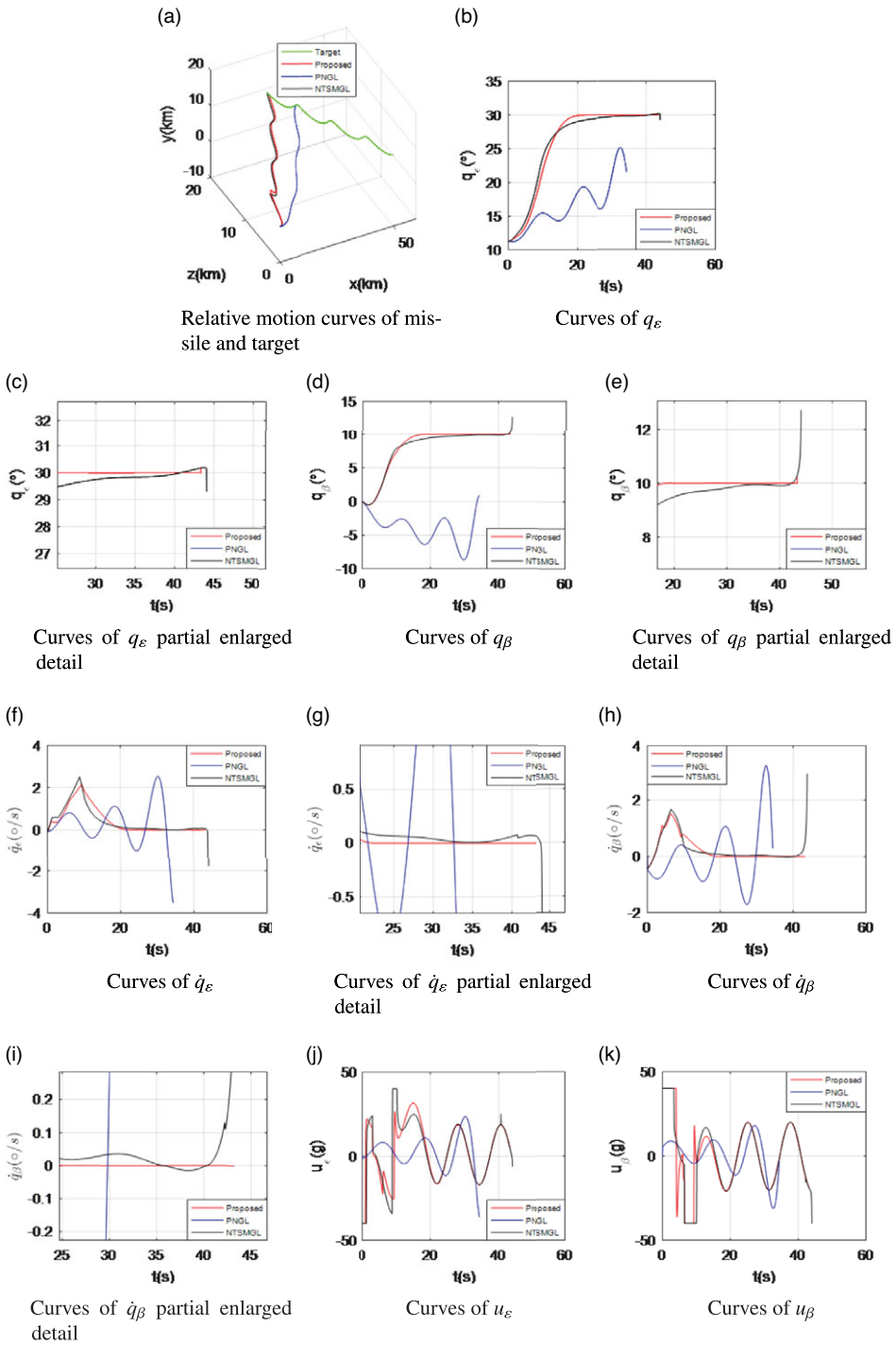
(a)

Relative motion curves of missile and target

(b)

Curves of q_ε

(c)

Curves of q_ε partial enlarged detail

(d)

Curves of q_β

(e)

Curves of q_β partial enlarged detail

(f)

Curves of $\dot{q}_\varepsilon$

(g)

Curves of $\dot{q}_\varepsilon$ partial enlarged detail

(h)

Curves of $\dot{q}_\beta$

(i)

Curves of $\dot{q}_\beta$ partial enlarged detail

(j)

Curves of u_ε

(k)

Curves of u_β

Figure 4. *Simulation results of three different guidance laws with Case 1.*

Table 5. *Simulation results of three different guidance laws with Case 1*

Guidance law	Miss distance(m)	Line-of-sight dip Angle error (°)	Line-of-sight drift Angle error (°)	Flight time(s)
Proposed	0.0014	0.0031	0.0054	43.334
PNGL	4.26	0.0059	8.39	34.419
NTSMGL	0.1571	0.0066	0.6963	44.079

NTSMGL can make the guidance system state converge in finite time and is robust to system disturbance. It can intercept manoeuvering targets.

After a lot of simulations, the control effect of u_{NTSMGL} is optimised by adjusting the parameters. Finally Select the guidance parameter of u_{NTSMGL} as $\beta = 10, p = 9, q = 7, k = 5.5, H = \begin{bmatrix} 0.01 & 0 \\ 0 & 0.01 \end{bmatrix}$.

For Case 1, when $a_{T\varepsilon} = 200 \sin(0.5t) \text{m/s}^2$, $a_{T\beta} = 200 \cos(0.5t) \text{m/s}^2$. Figure 4 and Table 5 reveal the simulation results of sinusoidal wave manoeuvering target interception under three different guidance laws, which are the proposed guidance law in this paper, the PNGL and the NTSMGL. The relative motion curves of the missile and the target under three different guidance laws are shown in Fig. 4(a). All three different guidance laws allow the missile to successfully intercept sinusoidal manoeuverable targets, even if the missiles' flight paths are different. Figure 4(b)–(e) shows the curves of q_ε, the curves of q_ε partial enlarged detail, the curves of q_β and the curves of q_β partial enlarged detail, respectively. It can be clearly seen from Fig. 4(b)–(e) that both the proposed guidance law in this paper and NTSMGL guarantee the convergence of q_ε and q_β. However, PNGL cannot ensure the convergence of q_ε and q_β. In addition, q_ε and q_β under the proposed guidance law in this paper obviously has faster convergence speed and higher accuracy than those under NTSMGL. Figure 4(f)–(i) shows the curves of $\dot{q}_\varepsilon$, the curves of $\dot{q}_\varepsilon$ partial enlarged detail, the curves of $\dot{q}_\beta$ and the curves of $\dot{q}_\beta$ partial enlarged detail, respectively. It can be clearly seen from Fig. 4(f)–(i) that the guidance law proposed in this paper makes $\dot{q}_\varepsilon$ and $\dot{q}_\beta$ converge to near zero with high accuracy. Although NTSMGL also makes $\dot{q}_\varepsilon$ and $\dot{q}_\beta$ converge to near zero, divergence phenomenon appears at the moment when the missile and the target are about to encounter. And PNGL does not makes $\dot{q}_\varepsilon$ and $\dot{q}_\beta$ converge to near zero. Figure 4(j)–(k) shows the curves of u_ε and u_β. The elevation and azimuth acceleration commands of the missile u_ε and u_β are in a reasonable range under three different guidance laws. From Table 5 it can be known that under the guidance law proposed in this paper, the missile's miss distance to the target is much smaller than the other two guidance laws. At the same time, the line-of-sight dip angle error and line-of-sight drift angle error are far less than the other two guidance laws. Compared with NTSMGL, the flight time of the missile under action of the guidance law proposed in this paper is shorter, which makes the interception probability of the missile with shorter flight time increase in the terminal guidance phase. Although the flight time of the missile under action of PNGL is the shortest, it cannot control the line-of-sight angle, and the miss distance is large. In conclusion, by comparing the simulation results of the three guidance laws, the guidance law proposed in this paper has better control performance.

For Case 2, when $a_{T\varepsilon} = -200 \text{m/s}^2$, $a_{T\beta} = 200 \text{m/s}^2$. Figure 5 and Table 6 reveal the simulation results of constant manoeuvering target interception under three different guidance laws, which are the proposed guidance law in this paper, the conventional PNGL and the NTSMGL. The relative motion curves of the missile and the target under three different guidance laws are shown in Fig. 5(a). PNGL failed to intercept the constant manoeuvering target, while the other two guidance laws succeeded. Figure 5(b)–(e) indicates the curves of q_ε, the curves of q_ε partial enlarged detail, the curves of q_β and the curves of q_β partial enlarged detail, respectively. Figure 5(f)–(i) displays the curves of $\dot{q}_\varepsilon$, the curves of $\dot{q}_\varepsilon$ partial enlarged detail, the curves of $\dot{q}_\beta$ and the curves of $\dot{q}_\beta$ partial enlarged detail, respectively. Figure 5(j)–(k) shows the curves of u_ε and u_β. Figure 5(b)–(k) shows the same situation as Fig. 4(b)–(k), so it will not be repeated here. It can be seen from Table 6 that, under the guidance law proposed in this paper, the miss distance of the missile to the target is much less than NTSMGL, while PNGL cannot intercept the
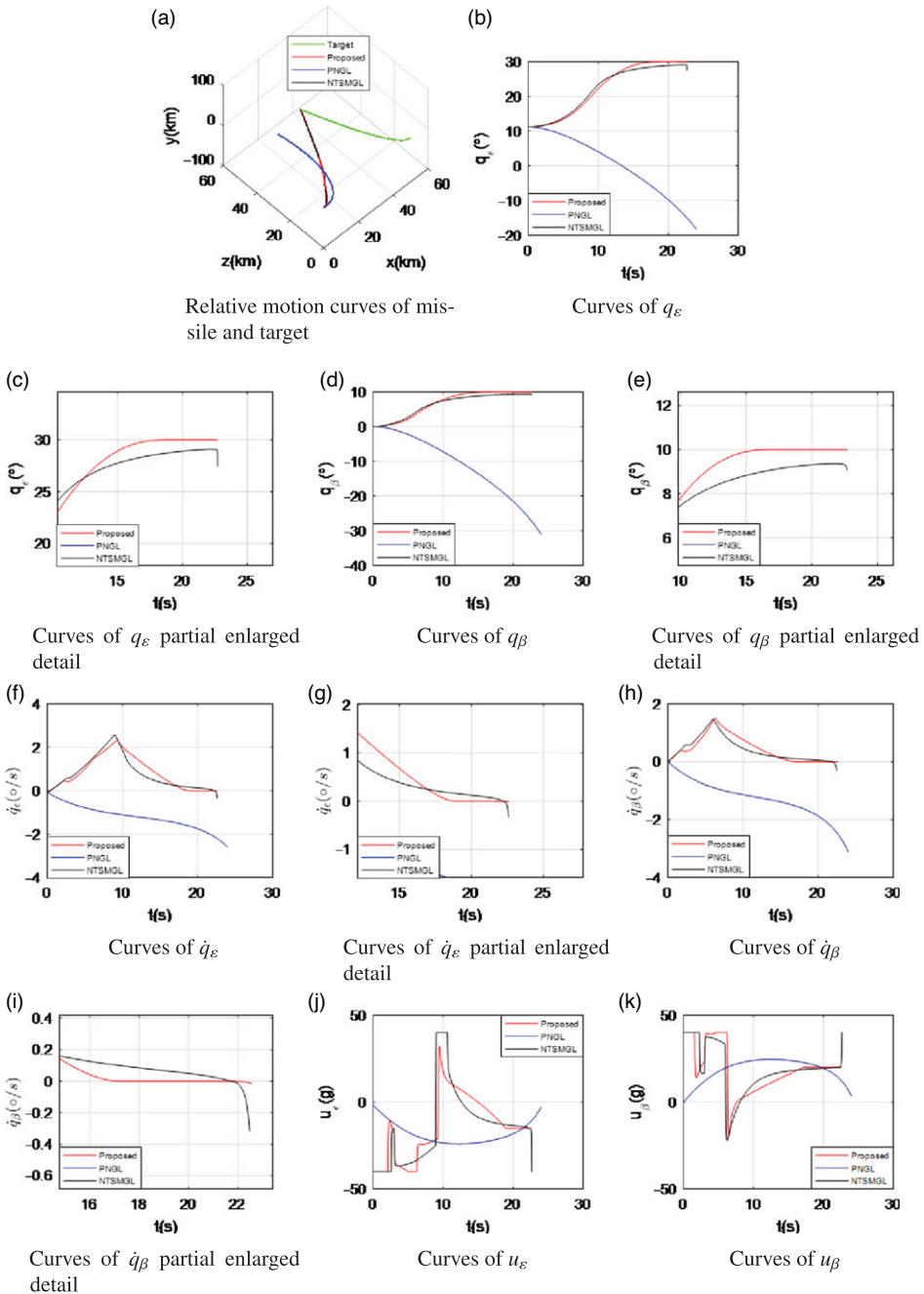
(a) Relative motion curves of missile and target

(b) Curves of q_ε

(c) Curves of q_ε partial enlarged detail

(d) Curves of q_β

(e) Curves of q_β partial enlarged detail

(f) Curves of $\dot{q}_\varepsilon$

(g) Curves of $\dot{q}_\varepsilon$ partial enlarged detail

(h) Curves of $\dot{q}_\beta$

(i) Curves of $\dot{q}_\beta$ partial enlarged detail

(j) Curves of u_ε

(k) Curves of u_β

Figure 5. *Simulation results of three different guidance laws with Case 2.*

constant manoeuver target with the acceleration of 20g. At the same time, the line-of-sight dip angle error and line-of-sight drift angle error under action of the guidance law proposed in this paper are far less than NTSMGL, while PNGL has no ability to control the line-of-sight angle. In conclusion, by comparing the simulation results of the three guidance laws, the guidance law proposed in this paper has better control performance.

Table 6. *Simulation results of three different guidance laws with Case 2*

Guidance law	Miss distance(m)	Line-of-sight dip Angle error (°)	Line-of-sight drift Angle error (°)	Flight time(s)
Proposed	7.7747e-06	0.0067	0.0084	22.702
PNGL	29481	48.1275	40.9223	23.999
NTSMGL	0.676	1.2262	1.7013	22.705

5.0 Conclusions

In this paper, a new sliding mode adaptive neural network guidance law is proposed to intercept highly manoeuvering targets with ideal impact angles. The guidance law, based on fast nonsingular terminal sliding mode, ensures that the line-of-sight angle and the line-of-sight angle rate converge in finite-time rather than asymptotically. A fast-power-reaching law is adopted to ensure the fast convergence of the sliding mode surface and overcome the chattering phenomenon of the sliding mode control. Aiming at the external disturbance caused by the target manoeuvering, the RBF neural network without the target prior information is proposed to estimate. At the same time, adopt the adaptive law to eliminate estimation errors of RBF neural network. According to Lyapunov stability theory, the proposed guidance law can ensure the guidance system stability. In order to verify the effectiveness of the proposed guidance law in this paper, the numerical simulation is carried out for four missiles with the same initial state intercepting 20g sine wave and constant two big manoeuvering target situation at different expected terminal line-of-sight angles. The numerical simulation results demonstrate that the proposed guidance law has small miss distance and line-of-sight angle error, so it has excellent control performance. In order to verify the superiority of the proposed guidance law in this paper, it is compared with the conventional PNGL and the NTSMGL. The numerical simulation is carried out for three different guidance laws that are used to intercept 20g sine wave and constant big manoeuvering target situation at desired terminal line-of-sight angles. The numerical simulation results demonstrate that the proposed guidance law is superior to the other two guidance laws in both miss distance and line-of-sight angles error control.

References

[1] Ben-Asger, J.Z., Farber, N. and Levinson, S. New proportional navigation law for ground-to-air systems, *J. Guidance Control Dyn.*, 2003, **26**, (5), pp 822–825.

[2] Gao, C., Li, J., Feng, T. and Jing, W. Adaptive terminal guidance law with impact-angle constraint, *Aeronaut. J.*, 2018, **122**, (1249), pp 369–389.

[3] Yang, C.D. and Yang, C.C. Analytical solution of three-dimensional realistic true proportional navigation, *J. Guidance Control Dyn.*, 1996, **19**, (3), pp 569–577.

[4] Chakravarthy, A. and Ghose, D. Capturability of realistic generalized true proportional navigation, *IEEE Trans.* Aerospace Electron. *Syst.*, 1996, **32**, (1), pp 407–418.

[5] Li, K.B., Zhang, T.T. and Chen, L. Ideal proportional navigation for exoatmospheric interception, *Chin. J. Aeronaut.*, 2013, **26**, (4), pp 976–985.

[6] Cho, N. and Kim, Y. Modified pure proportional navigation guidance law for impact time control, *J. Guidance Control Dyn.*, 2016, **39**, (4), pp 852–872.

[7] Cho, N., Kim, Y. and Park, S. Three-dimensional nonlinear differential geometric path-following guidance law, *J. Guidance Control Dyn.*, 2015, **38**, (12), pp 2366–2385.

[8] Fu, S.N., Liu, X.D., Zhang, W.J. and Xia, Q.L. Multiconstraint adaptive three-dimensional guidance law using convex optimisation, *J. Syst. Eng. Electron.*, 2020, **31**, (4), pp 791–803.

[9] He, S.M., Wang, W. and Wang, J. Three-dimensional impact angle guidance laws based on model predictive control and sliding mode disturbance observer, *J. Dyn. Syst. Meas. Controls*, 2016, **138**, (8), pp 1–8.

[10] Li, G.L. and Ji, H.B. A three-dimensional robust nonlinear terminal guidance law with ISS finite-time convergence, *Int. J. Control*, 2016, **89**, (5), pp 938–949.

[11] Man, C.Y., Liu, R.J. and Li, S.H. Three-dimensional suboptimal guidance law based on theta - D technique and nonlinear disturbance observer, *J. Aerospace Eng.*, 2019, **233**, (14), pp 5122–5133.

[12] Weiss, G. and Rusnak, I. All-aspect three-dimensional guidance law based on feedback linearisation, *J. Guidance Control Dyn.*, 2015, 38, (12), pp 2421–2428.

[13] Yan, X.H., Zhu, J.H., Kuang, M.C. and Yuan, X.M. A computational-geometry-based 3-dimensional guidance law to control impact time and angle, *Aerospace Sci. Technol.*, 2020, **98**, pp 1–12.

[14] Ji, Y., Lin, D.F., Wang, W., Hu, S.Y. and Pei, P. Three-dimensional terminal angle constrained robust guidance law with autopilot lag consideration, *Aerospace Sci. Technol.*, 2020, **86**, pp 160–176.

[15] Shafiei, M.H. and Vazirpour, N. The approach of partial stabilisation in design of discrete-time robust guidance laws against manoeuvering targets, *Aeronaut. J.*, 2020, **124**, (1277), pp 1114–1127.

[16] Guo, J., Li, Y. and Zhou, J. A new continuous adaptive finite time guidance law against highly manoeuvering targets, *Aerospace Sci. Technol.*, 2019, **85**, pp 40–47.

[17] Li, K.-B., Shin, H.-S. and Tsourdos, A. Capturability of a sliding-mode guidance law with finite-time convergence, *IEEE Trans.* Aerospace Electron. *Syst.*, 2020, **56**, (3), pp 2312–2325.

[18] Zhang, W.J., Xia, Q.L. and Li, W. Novel second-order sliding mode guidance law with an impact angle constraint that considers autopilot lag for intercepting manoeuvering targets, *Aeronaut. J.*, 2020, **124**, (1279), pp 1350–1370.

[19] He, S.M., Lin, D.F. and Wang, J. Continuous second-order sliding mode based impact angle guidance law, *Aerospace Sci. Technol.*, 2015, **41**, pp 199–208.

[20] Sun, L., Wang, W., Yi, R. and Xiong, S. A novel guidance law using fast terminal sliding mode control with impact angle constraints, *ISA Trans.*, 2016, **64**, pp 12–23.

[21] Song, J., Song, S. and Zhou, H. Adaptive nonsingular fast terminal sliding mode guidance law with impact angle constraints, *Int. J. Control Autom. Syst.*, 2016, **14**, (1), pp 99–114.

[22] He, S. and Lin, D. Sliding mode-based continuous guidance law with terminal angle constraint, *Aeronaut. J.*, 2016, **120**, (1229), pp 1175–1195.

[23] Wu, K., Cai, Z.H., Zhao, J. and Wang, Y.X. Target tracking based on a nonsingular fast terminal sliding mode guidance law by fixed-wing UAV, *Appl. Sci.*, 2017, **7**, (4), pp 1–18.

[24] Zhao, Z.H., Li, C.T., Yang, J. and Li, S.H. Output feedback continuous terminal sliding mode guidance law for missile-target interception with autopilot dynamics, *Aerospace Sci. Technol.*, 2019, **86**, pp 256–267.

[25] Xu, S., Gao, M., Fang, D., Wang, Y. and Li, B.C. A novel adaptive second-order nonsingular terminal sliding mode guidance law design, *J. Aerospace Eng.*, 2020, **234**, (16), pp 2263–2273.

[26] Zhang, W.J., Fu, S.N., Li, W. and Xia, Q.L. An impact angle constraint integral sliding mode guidance law for manoeuvering targets interception, *J. Syst. Eng. Electron.*, 2020, **31**, (1), pp 168–184.

[27] Song, J.H. and Song, S.M. Three-dimensional guidance law based on adaptive integral sliding mode control, *Chin. J. Aeronaut.*, 2016, 29, (1), pp 202–214.

[28] Meng, K.Z. and Zhou, D. Super-twisting integral-sliding-mode guidance law considering autopilot dynamics, *J. Aerospace Eng.*, 2018, 232, (9), pp 1787–1799.

[29] Kumar, S.R. and Ghose, D. Three-dimensional impact angle guidance with coupled engagement dynamics, *J. Aerospace Eng.*, 2017, 231, (4), pp 621–641.

[30] Zhang, N., Gai, W.D., Zhong, M.Y. and Zhang, J. A fast finite-time convergent guidance observer for unmanned aerial vehicles law with nonlinear disturbance collision avoidance, *Aerospace Sci. Technol.*, 2019, **86**, pp 204–214.

[31] Zhao, F.J. and You, H. New three-dimensional second-order sliding mode guidance law with impact-angle constraints, *Aeronaut. J.*, 2019, **124**, (1273), pp 368–384.

[32] Yang, F. and Xia, G. A finite-time 3D guidance law based on fixed-time convergence disturbance observer, *Chin. J. Aeronaut.*, 2020, **33**, (4), pp 1299–1310.

[33] Ma, K.M., Khalil, H.K. and Yao, Y. Guidance law implementation with performance recovery using an extended high-gain observer, *Aerospace Sci. Technol.*, 2013, **24**, (1), pp 177–186.

[34] Chwa, D. Robust nonlinear disturbance observer based adaptive guidance law against uncertainties in missile dynamics and target maneuver, *IEEE Trans.* Aerospace Electron. *Syst.*, 2018, **54**, (4), pp 1739–1749.

[35] Lin, C.L., Hsieh, S.L. and Lin, Y.P. Trajectory estimation based on extended state observer with Fal-filter, *Aeronaut. J.*, 2015, **119**, (1218), pp 1017–1031.

[36] Zhao, E.J., Chao, T., Wang, S.Y. and Yang, M. Multiple flight vehicles cooperative guidance law based on extended state observer and finite time consensus theory, *J. Aerospace Eng.*, 2018, **232**, (2), pp 270–279.

[37] Duan, M.J., Zhou, D. and Cheng, D.L. Extended state observer-based finite-time guidance laws on account of thruster dynamics, *J. Aerospace Eng.*, 2019, **233**, (12), pp 4583–4597.

[38] Liao, F., Luo, Q., Ji, H.B. and Gai, W. Guidance laws with input saturation and nonlinear robust H-infinity observers, *ISA Trans.*, 2016, **63**, pp 20–31.

[39] Si, Y. and Song, S. Adaptive reaching law based three-dimensional finite-time guidance law against manoeuvering targets with input saturation, *Aerospace Sci. Technol.*, 2017, **70**, pp 198–210.

[40] Si, Y. and Song, S. Three-dimensional adaptive finite-time guidance law for intercepting manoeuvering targets, *Chin. J. Aeronaut.*, 2017, **30**, (6), pp 1985–2003.

[41] Jiang, Y., Wang, Q. and Dong, C. A reaching law based neural network terminal sliding-mode guidance law design, TENCON 2013-2013 IEEE Region 10 Conference (31194), 2013.